

ARTICLE

Open Access

# Merging of relaxations and step-like increase of accompanying supercooled liquid region in metallic glasses via ultrafast nanocalorimetry

Meng Gao <sup>1,2</sup> and John H. Perepezko<sup>2</sup>

## Abstract

Glassy materials under external stimuli usually display multiple and complex relaxations. The relaxations and the evolution paths of glassy materials significantly affect their properties and are closely related to many key issues in glass physics, such as glass transition and thermoplastic forming. However, until now, the relaxation dynamics in the presence of external stimuli and the microscopic atomic motion of glassy materials have been unclear due to the lack of structural information. By combining Flash and conventional differential scanning calorimetry (DSC), we applied a very large range of heating rate of six orders of magnitude and investigated the relaxation dynamics of three typical metallic glasses. We discovered the merging of distinct relaxation events with increasing rate of heating. Most interestingly, the experiments revealed new behaviors with step-like increases in the supercooled liquid region and excess heat capacity during the merging of multiple relaxations. A comprehensive scheme was proposed for the evolution of the thermal relaxation spectrum, the heterogeneity of the corresponding atomic motion and the potential energy landscape with rate of heating. These experimental results shed light on the mechanism of atomic rearrangement during heating and provided a new approach to regulate the physical properties of amorphous materials by controlling their intrinsic relaxation dynamics.

## Introduction

The relaxation phenomena of metallic glasses (MGs) have attracted a great deal of attention from researchers who seek to unveil the nature of the glass transition and other key issues in glass physics, such as physical aging, the memory effect and thermoplastic forming<sup>1–5</sup>. Compared to their crystalline counterparts, MGs display diverse relaxation modes over wide ranges of temperature and timescale, such as the primary  $\alpha$  relaxation, the secondary  $\beta$  (Johari-Goldstein) relaxation and the faster relaxation modes called  $\beta'$  or  $\gamma$  relaxations (shown in the upper part of Fig. 1a)<sup>6–11</sup>. Different relaxation modes gradually decouple during vitrification. At a sufficiently

high temperature, there is only the  $\alpha$  relaxation; when the liquid quickly quenches into the supercooled liquid region, the relaxation mode splits into  $\alpha$  and  $\beta$  relaxations. In the glass state below the glass transition temperature, the  $\alpha$  relaxation disappears, and the relaxation mode further decouples into  $\beta$  and  $\beta'$  relaxations<sup>5,12</sup>. However, few studies have focused on the evolution of the relaxation mode during the glass-to-liquid transition (GLT) by fast heating to bypass crystallization<sup>13–16</sup>. From the view of practical applications, the GLT process is one of the critical issues in the net-shape thermoplastic forming processes of MGs, such as injection molding, blow molding, and microreplication<sup>14,17,18</sup>. Meanwhile, researchers have recently reported that the macroscopic GLT is induced by the activation and percolation of numerous flow units that are closely correlated with local  $\beta$  and  $\beta'$  relaxations<sup>9,15</sup>. Thus, understanding how atomic rearrangements govern these relaxation processes and the detailed evolution paths of different relaxations is of

Correspondence: Meng Gao (gaomeng@nimte.ac.cn)

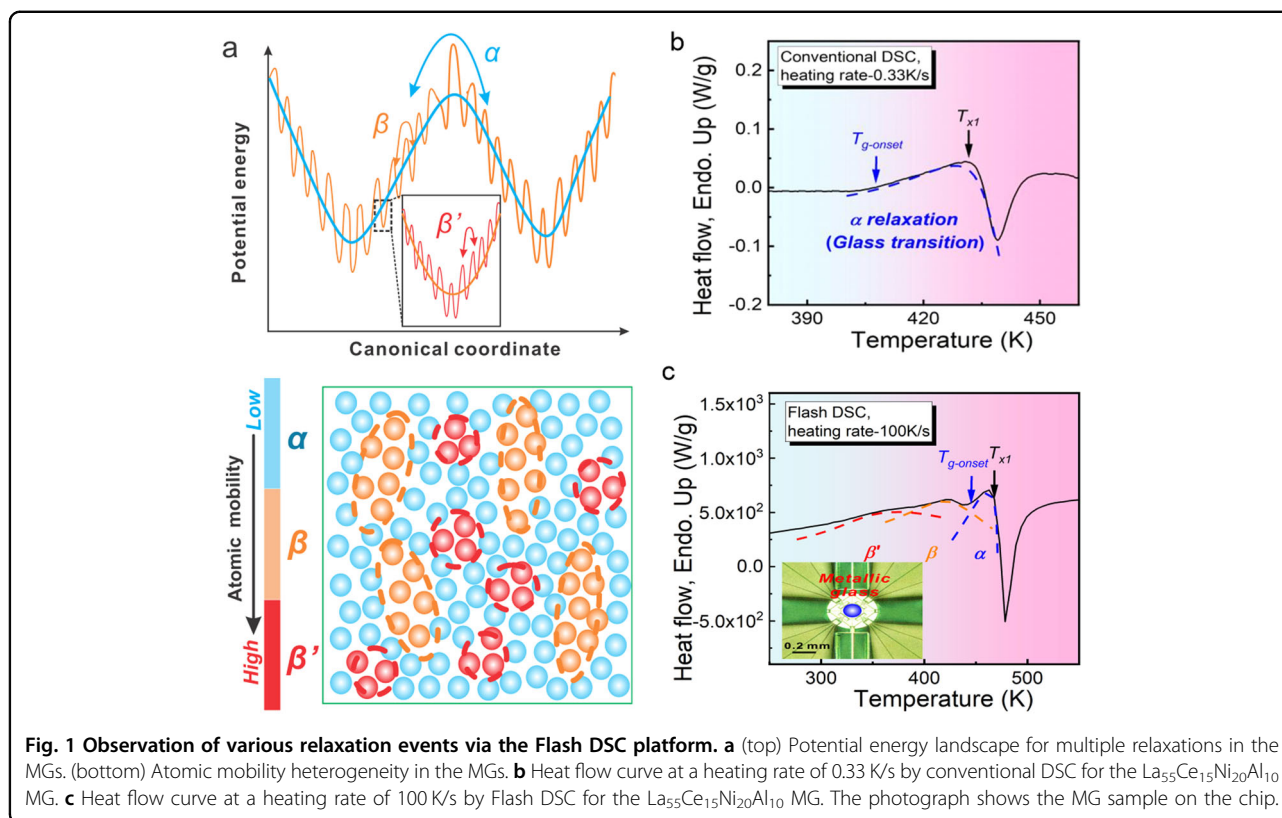
<sup>1</sup>CAS Key Laboratory of Magnetic Materials and Devices, and Zhejiang Province Key Laboratory of Magnetic Materials and Application Technology, Ningbo Institute of Materials Technology & Engineering, Chinese Academy of Sciences, Ningbo, Zhejiang 315201, China

<sup>2</sup>Department of Materials Science and Engineering, University of Wisconsin-Madison, Madison, WI 53706, USA

© The Author(s) 2022



**Open Access** This article is licensed under a Creative Commons Attribution 4.0 International License, which permits use, sharing, adaptation, distribution and reproduction in any medium or format, as long as you give appropriate credit to the original author(s) and the source, provide a link to the Creative Commons license, and indicate if changes were made. The images or other third party material in this article are included in the article's Creative Commons license, unless indicated otherwise in a credit line to the material. If material is not included in the article's Creative Commons license and your intended use is not permitted by statutory regulation or exceeds the permitted use, you will need to obtain permission directly from the copyright holder. To view a copy of this license, visit <http://creativecommons.org/licenses/by/4.0/>.



great importance in fundamental research and practical applications for MGs.

For thermal activation processes in MGs, such as crystallization and different relaxations, including the primary  $\alpha$  relaxation, the relationship between the typical temperature (crystallization temperature or glass transition temperature) and the heating rate roughly follows the Kissinger equation or the Arrhenius equation<sup>9,10,19–22</sup>. Thus, different thermal activation processes can be separated under high heating rates. For example, the hidden glass transition ( $\alpha$  relaxation) in marginal Al-based MGs has been separated from primary crystallization, and the weak  $\beta$  relaxation in fragile MGs is separated from the  $\alpha$  relaxation when the heating rate reaches a critical value<sup>19,20</sup>. Furthermore, the activation processes of different relaxations during the GLT with increasing temperature in MGs are usually accompanied by obvious thermal signals, such as endothermic peaks before the glass transition, which usually correspond to the appearance of  $\beta$  and  $\beta'$  relaxations and the unfreezing of the corresponding local regions<sup>9,15,16,20</sup>. Considering that the activation energies of  $\beta$  and  $\beta'$  relaxations are much smaller than that of the  $\alpha$  relaxation, a relaxation mode coupling should appear for different relaxations with increasing heating rates. Moreover, recent studies have established that the secondary  $\beta$  relaxations in MGs are governed by string-like clusters of particles with

cooperative motion<sup>23,24</sup> and that fast  $\beta'$  or  $\gamma$  relaxations result from caging-breaking motion driven by internal stress in nonequilibrium states (shown in the lower part of Fig. 1a)<sup>9,10,25,26</sup>. Therefore, the above possible relaxation mode coupling with increasing rate of heating may imply the coupling of various atomic rearrangement motions, which provides critical information for understanding hidden physical process during the GLT. However, due to the limited experimental capacity of calorimetry instruments, until now, there has been no report about this kind of mode coupling for different relaxation events with heating. Recently, one advanced commercial chip-based instrument for fast differential scanning calorimetry (DSC) (Mettler Toledo, Flash DSC) enabled the use of heating rates for thermoanalytical measurements over a range of six orders of magnitude, which provides a good opportunity to systematically study relaxation events during heating and related relaxation dynamics in amorphous materials<sup>27–30</sup>.

In this paper, we systematically investigate the relaxation dynamics of three typical MG systems with different relaxation patterns in a large range of heating rates, six orders of magnitude, by combining advanced Flash and conventional DSC instruments. First, we find the step-like emergence of three distinct relaxation events as the temperature and heating rate increase in a LaCe-based MG system. Moreover, we observe and discover a large

increase in the supercooled liquid region during the merging of multiple relaxations. Additionally, the corresponding excess heat capacity exhibits a similar step-like increase with the merging of multiple relaxations. In addition, similar relaxation merging behaviors with heating rate take place in the other two MG systems. These results reveal the novel activation path of different relaxation events during the GLT with the heating rate and provide a new approach to tune the relaxation dynamics by ultrafast heating to increase the supercooled liquid region.

## Materials and methods

### Materials

Ingots of  $\text{La}_{55}\text{Ce}_{15}\text{Ni}_{20}\text{Al}_{10}$ ,  $\text{La}_{60}\text{Ni}_{25}\text{Al}_{15}$  and  $\text{Al}_{90}\text{Ca}_{10}$  were prepared by arc melting the elemental components several times in a Ti-gettered argon atmosphere to ensure homogeneity. Then, ribbon samples were prepared by single-roller melt spinning on a copper wheel with a tangential speed of 55 m/s. The ribbons had a cross section of approximately  $2\text{ mm} \times 20\text{ }\mu\text{m}$  and were approximately several meters in length. The cooling rates for preparing the ribbon-like samples in this study were estimated as approximately  $2.5 \times 10^6\text{ K/s}$ . The glassy nature for all ribbon-like samples was ascertained by X-ray diffraction (D8 Discover Diffraction with  $\text{Cu } K_{\alpha}$  radiation, Bruker, United States) and DSC (Diamond DSC, PerkinElmer Inc., United States).

### Calorimetry measurements

The samples for all the DSC tests, including conventional DSC and Flash DSC tests, were cut from the above as-cast ribbons in sizes that were suitable for different DSC instruments. A high-rate differential scanning calorimeter with chip sensors (Flash DSC 2, with maximum heating and cooling rates of  $4 \times 10^4$  and  $1 \times 10^4\text{ K/s}$ , respectively, Mettler Toledo, Switzerland) was used to investigate the thermal behaviors of various MG systems under different heating rates from 5 K/s to 10,000 K/s. The measurement temperature range for the Flash DSC 2 was between  $-90\text{ }^{\circ}\text{C}$  and  $1000\text{ }^{\circ}\text{C}$ . The as-cast ribbon-like samples were cut into tiny rectangular pieces of approximately  $150\text{ }\mu\text{m} \times 150\text{ }\mu\text{m} \times 20\text{ }\mu\text{m}$  (length  $\times$  width  $\times$  thickness) and then loaded onto the Flash DSC chip. As a reference, the heat flow curve at a low heating rate of 0.33 K/s was also measured by Diamond DSC in this study. For conventional DSC tests, the as-cast ribbon-like samples were cut into small pieces by scissors; each piece was approximately  $5\text{ mm} \times 2\text{ mm} \times 20\text{ }\mu\text{m}$  (length  $\times$  width  $\times$  thickness), which was suitable to be loaded into an aluminum pan for conventional DSC measurements. The masses of the samples in conventional DSC measurements were weighed. For the mass of the tiny Flash DSC samples, the mass was estimated from the corresponding volume

(measured by optical microscope) and density (estimated by the Archimedean technique).

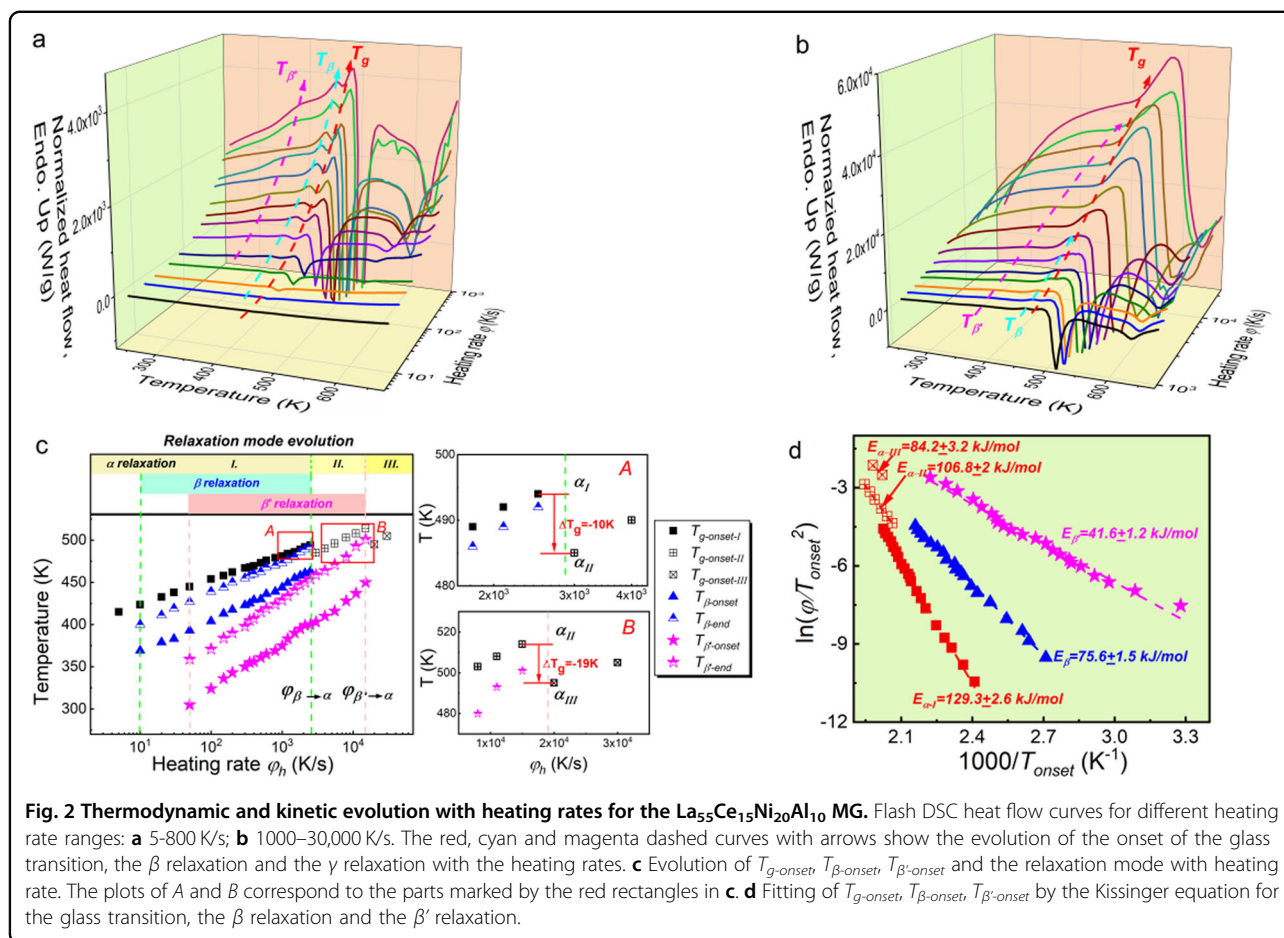
### Heat capacity measurement based on the Flash DSC platform and confirmation of excess heat capacity at the glass transition temperature

Based on the Flash DSC platform, the heat capacity  $c_p$  was measured<sup>31</sup>. The detailed temperature–time program for the step response analysis included a temperature jump of 2 K (far less than the thermal fluctuations) at one heating rate  $\varphi_h$  and isotherms of duration  $\Delta t$ . The value of  $\Delta t$  was set to guarantee a frequency of 10 Hz. Thus, for different applied heating rates, the value of  $\Delta t$  was adjusted. The complex heat capacity,  $c_p^*(\omega) = c_p'(\omega) - ic_p''(\omega)$ , was calculated by a Fourier transform of the heat flow rate  $HF(t)$  and the instantaneous heating rate  $\varphi_h(t)$ , 
$$c_p^*(\omega) = \frac{\int_0^{\omega} HF(t)e^{-i\omega t} dt}{\int_0^{\omega} \varphi_h(t)e^{-i\omega t} dt}$$
, where  $c_p^*$  is the complex heat capacity,  $c_p'$  and  $c_p''$  are the real part and imaginary part of the complex heat capacity,  $\omega$  is the frequency,  $HF$  is the heat flow and  $\varphi_h$  is the heating rate. From the obtained complex heat capacity, the reversible heat capacity  $c_p$  was calculated by  $c_p(\omega) = (c_p'(\omega)^2 + c_p''(\omega)^2)^{0.5}$ . For each applied heating rate  $\varphi_h$ , the temperature of the onset of the glass transition was obtained from the corresponding heat flow curve. Then, the excess heat capacity  $\Delta c_p$  at the glass transition temperature was calculated by subtracting the linear fit of the heat capacities of the supercooled liquid state and glass state.

## Results

### Observation of multiple relaxation events via the combined DSC platform in LaCe-based MG

Two typical heat flow curves by conventional DSC with a heating rate of 0.33 K/s and by Flash DSC with a heating rate of 100 K/s for the LaCe-based MG are exhibited in Fig. 1b, c, respectively. The conventional heat flow curve displays only the glass transition signal corresponding to the primary  $\alpha$  relaxation. In contrast, the Flash DSC heat flow curve exhibits two distinct endothermic peaks before the glass transition. For LaCe-based MG, the primary  $\alpha$  relaxation, the secondary  $\beta$  relaxation and the fast  $\beta'$  relaxation have been reported based on results of dynamic mechanical analysis (DMA)<sup>9</sup>. However, the conventional calorimetry method with limited heating rates of several K/s cannot observe the activation of the secondary  $\beta$  relaxation and the fast  $\beta'$  relaxation except when the thermal signal of secondary  $\beta$  relaxation is induced by a thermal annealing treatment<sup>32,33</sup>. By comparison, in this study, based on ultrafast Flash DSC, the secondary  $\beta$  relaxation and the fast  $\beta'$  relaxation are observed for the first time by the calorimetry method, as shown in Fig. 1c. Previous studies have reported that the secondary



$\beta$  relaxation and fast  $\beta'$  relaxation commonly observed in rare earth-based MGs are separately correlated to string-like motion and more local cage-breaking motion, which can be attributed to the presence of highly ‘mobile’ atomic pairs, such as the rare earth element–Ni pair<sup>9,10,16</sup>. Therefore, from this perspective, ultrafast nanocalorimetry provides a new and powerful tool to investigate dynamic behaviors in glasses, such as the GLT and various relaxation behaviors during heating, and the accompanying local atomic rearrangement motions during these thermally activated processes in glassy materials.

To investigate the evolution of various relaxation events with heating rates in the LaCe-based MG, a series of heating rates ranging over six orders of magnitude were applied to measure the corresponding heat flow curves. All heat flow curves were normalized by sample mass and are shown in Fig. 2a, b. From Fig. 2a, b, when the heating rate  $\varphi_h$  increased to approximately 10 K/s and 50 K/s, the thermal signals of the endothermic peaks for the secondary  $\beta$  relaxation and fast  $\beta'$  relaxation appeared, respectively. Considering that the thermal signals for the secondary  $\beta$  relaxation and fast  $\beta'$  relaxation correspond to the activation of local string-like and cage-breaking

motions, as shown in Fig. 1a, the thermal signal intensity was relatively weak, and it was difficult to detect these signals at low heating rates by conventional DSC instruments<sup>20</sup>. In contrast, when the heating rates were larger than the corresponding critical heating rates for the appearance of the  $\beta$  and  $\beta'$  relaxations, the thermal signals corresponding to the activation of the  $\beta$  and  $\beta'$  relaxations were strong enough to be observed by Flash DSC; they appear as two obvious endothermic peaks before the glass transition in Fig. 1c. From the perspective of recovery enthalpy during heating, when the heating rate is very small, the effect of the decrease in the recovery enthalpy induced by structural relaxation during heating is very large, and the thermal signals from the  $\beta$  and  $\beta'$  relaxations are relatively weak. When the applied heating rates become large enough, the effect of the decrease in the recovery enthalpy can be minimized, and thus, the thermal signals from the  $\beta$  and  $\beta'$  relaxations become strong enough to be detected<sup>16,20</sup>. Moreover, it is apparent that the thermal signals for the primary  $\alpha$  relaxation (glass transition), the secondary  $\beta$  relaxation and the fast  $\beta'$  relaxation evolve with increasing rate of heating. In particular, it is intriguing to observe in Fig. 2b that the

secondary  $\beta$  relaxation started to merge with the primary  $\alpha$  relaxation when the heating rate increased into one critical value  $\varphi_{\beta \rightarrow \alpha}$  of approximately 2400 K/s. The merging of the initial  $\alpha$  relaxation (marked as  $\alpha_I$ ) and the secondary  $\beta$  relaxation led to the second stage of the  $\alpha$  relaxation (marked as  $\alpha_{II}$ ). Furthermore, when the heating rate continued to increase to another critical value  $\varphi_{\beta' \rightarrow \alpha}$  of approximately 15,000 K/s, the fast  $\beta'$  relaxation merged with the  $\alpha_{II}$  relaxation and entered the third stage of  $\alpha$  relaxation (marked as  $\alpha_{III}$ ). Therefore, the above results directly show that the thermal relaxation spectra for MGs at different heating rate ranges are not the same and that there appear to be different activated relaxation modes for one MG system within different heating rate ranges.

#### Activation energies for various relaxation events

To further illustrate the evolution paths of the different relaxation events for LaCe-based MG, the detailed evolutions of the onset temperature  $T_{onset}$  and the end temperature  $T_{end}$  for the different relaxation events with heating rates were obtained based on Fig. 2a, b and plotted in Fig. 2c. The  $\alpha$  relaxation process within the whole experimental heating rate range clearly displayed three stages: stage I (heating rate below 2400 K/s), stage II (heating rate between 2400 K/s and 15,000 K/s) and stage III (heating rate above 15,000 K/s). When the heating rate increased to 2400 K/s, the end temperature of the secondary  $\beta$  relaxation reached the onset temperature of the  $\alpha$  relaxation, which implied the merging of the secondary  $\beta$  relaxation and  $\alpha$  relaxation (shown in the upper-right plot of A in Fig. 2c). When the heating rate increased to 15,000 K/s, the end temperature of the fast  $\beta'$  relaxation reached the onset temperature of the  $\alpha$  relaxation, which implied the merging of the fast  $\beta'$  relaxation and the  $\alpha$  relaxation (shown in the lower-right plot of B in Fig. 2c).

Notably, the shift of all three relaxations to higher temperatures with increasing heating rate in Fig. 2a and b directly implied that these relaxations were thermally activated processes. Although the representation of the temperature and heating rate dependence has been presented differently in the literatures<sup>9,10,20–22</sup>, such as the Kissinger equation or Arrhenius equation, the values of the effective activation energy for the relationships obtained by fitting the Kissinger equation and Arrhenius equation within a small temperature range were very close<sup>20,34</sup>. Thus, in this study, the effective activation energy for relaxations was obtained by simply fitting the onset values of the relaxation events in Fig. 2c by the Kissinger equation, as shown in Fig. 2d. The values of the effective activation energies for the  $\alpha$ ,  $\beta$  and  $\beta'$  relaxations were  $129.3 \pm 2.6$ ,  $75.6 \pm 1.5$  and  $41.6 \pm 1.2$  kJ/mol ( $1.34 \pm 0.03$ ,  $0.78 \pm 0.02$  and  $0.43 \pm 0.01$  eV), respectively, which were consistent with the previous results obtained by the DMA method for LaCe-based MG<sup>9</sup>. Moreover, two step-like decreases in the

onset temperature for the  $\alpha$  relaxation were observed, 10 K and 19 K, when the  $\beta$  and  $\alpha$  relaxations merged and the  $\beta'$  and  $\alpha$  relaxations merged (shown in the right plots of Fig. 2c). Meanwhile, the corresponding activation energies for the  $\alpha$  relaxation showed two step-like decreases, from  $129.3 \pm 2.6$  kJ/mol ( $1.34 \pm 0.03$  eV) to  $106.8 \pm 2$  kJ/mol ( $1.11 \pm 0.02$  eV) and from  $106.8 \pm 2$  kJ/mol ( $1.11 \pm 0.02$  eV) to  $84.2 \pm 3.2$  kJ/mol ( $0.87 \pm 0.03$  eV). Thus, for the three stages of the  $\alpha$  relaxation, the corresponding activation energies differed. These results indicated that the  $\alpha$  relaxation was more easily activated at a large heating rate than a slow heating rate, considering the decrease in the  $\alpha$  relaxation activation energy with heating rate.

#### Supercooled liquid region evolution with heating rates

In general, for glassy materials, the glass transition behavior during heating (the GLT process) can be characterized by a single endothermic reaction, where the specific heat,  $c_p$ , increases abruptly to a maximum value and then remains constant or slightly decreases to the crystallization onset temperature,  $T_x$ . The temperature range between the glass transition and crystallization is called the supercooled liquid region ( $\Delta T = T_x - T_g$ ), which is closely related to glass formation ability and thermoplastic deformation ability. Moreover, considering the different evolution paths for the glass transition and crystallization with temperature during heating, the supercooled liquid region should continuously change with heating rate. Here, from Fig. 2c, the extent of the supercooled liquid region  $\Delta T$  for LaCe-based MG is plotted against the heating rate in Fig. 3a. The supercooled liquid region displays three stages: I, II and III, which are consistent with the three stages of the  $\alpha$  relaxation in Fig. 2c. When the heating rate was below 2400 K/s,  $\Delta T$  slowly increased with increasing heating rate; and when the heating rate increased to 2400 K/s,  $\Delta T$  exhibited an obvious step-like increase from 20 K to 70 K. Similarly, when the heating rate was between 2400 K/s and 15,000 K/s,  $\Delta T$  slowly increased with the heating rate; when the heating rate increased to 15,000 K/s,  $\Delta T$  developed a second step-like increase from 70 K to 110 K. The inserted graphs in Fig. 3a give the thermal relaxation spectrum corresponding to heating rates of 800 and 3000 K/s. Most interestingly, these two step-like increases in  $\Delta T$  were accompanied by the merging of the secondary  $\beta$  relaxation and  $\alpha$  relaxation and the merging of the fast  $\beta'$  relaxation and  $\alpha$  relaxation, respectively. For MGs, the larger the supercooled liquid region is, the greater the resistance to crystallization, which is one of the prerequisites for thermoplastic forming applications<sup>17</sup>.

#### Excess heat capacity evolution with heating rates

From the perspective of statistical physics, the heat capacity of matter in an equilibrium state reflects the possible motions of the basic atoms in the system<sup>35</sup>.

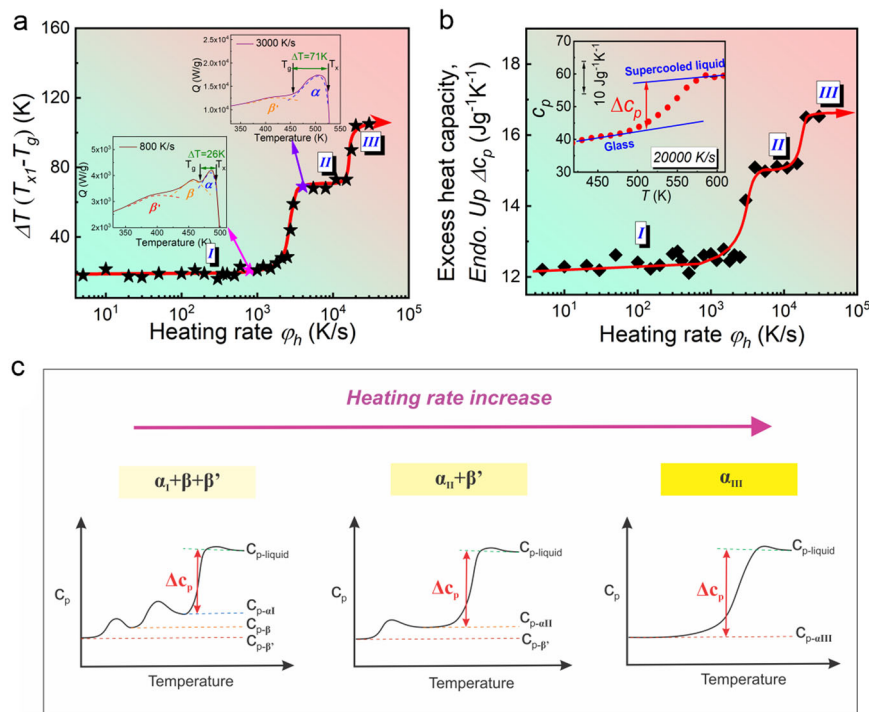


**Fig. 3** Evolution of the supercooled liquid region and excess heat capacity with heating rates for the  $\text{La}_{55}\text{Ce}_{15}\text{Ni}_{20}\text{Al}_{10}$  MG. **a** Evolution of the supercooled liquid region  $\Delta T$  with heating rate  $\phi_h$  indicated by the red curve. The inserted graphs show the thermal relaxation spectrum corresponding to heating rates of 800 and 3000 K/s. **b** The evolution of the excess heat capacity  $\Delta c_p$  with heating rate  $\phi_h$  indicated by the red curve. The inset plot gives the determination of the excess heat capacity at a heating rate of 20,000 K/s. **c** Scheme of the evolution of the heat capacity curve and relaxation mode with increasing heating rate.

Compared to the absolute heat capacity for one state, the excess heat capacity  $\Delta c_p$  of supercooled liquids relative to their glassy state contains contributions from the influence of changes in configuration states on the thermodynamic contributions of atomic rearrangement processes, which also give rise to secondary relaxations below the glass transition<sup>36–39</sup>. Thus, the excess heat capacity between the glass and liquid can reveal the kinds of atomic rearrangement motions that are involved in dynamic processes. Here, the heat capacities corresponding to different heating rates for LaCe-based MG were measured (discussed in detail in the Methods section), and one heat capacity curve for 20,000 K/s is shown in the inset of Fig. 3b. The excess heat capacity between the glassy state and the supercooled liquid state with different heating rates is plotted in Fig. 3b. Similar to the step-like increase in the supercooled liquid region, the excess heat capacity displayed two step-like increases with the merging of multiple relaxations. For stage I, before the  $\beta$  relaxation merged into the  $\alpha$  relaxation, the value of  $\Delta c_p$  was almost constant,  $12.4 \pm 0.3 \text{ Jmol}^{-1}\text{K}^{-1}$ . For MGs with only the thermal  $\alpha$  relaxation, previous studies reported that the values of excess heat capacity were almost constant,  $13.7 \pm 2.1 \text{ Jmol}^{-1}\text{K}^{-1}$ <sup>38,39</sup>, which was consistent

with the above results of stage I in this study. After the merging of the  $\beta$ ,  $\beta'$  relaxations and  $\alpha$  relaxation in stages II and III, the values of  $\Delta c_p$  jumped to  $15 \pm 0.1 \text{ Jmol}^{-1}\text{K}^{-1}$  and  $16.5 \pm 0.1 \text{ Jmol}^{-1}\text{K}^{-1}$ , respectively. This behavior can be used to understand the possible atomic rearrangement motions during the GLT. When the heating rate was in stage I, only the atomic rearrangement motions related to the  $\alpha$  relaxation contributed to the GLT. When the heating rate increased into stage II, both rearrangement motions related to the  $\alpha$  and  $\beta$  relaxations contributed to the GLT. When the heating rates further increased into stage III, all the rearrangement motions related to the  $\alpha$ ,  $\beta$  and  $\beta'$  relaxations participated in the GLT.

### Two additional typical MG systems

For MGs, the relaxation patterns are closely related to their chemical compositions and structural heterogeneities. Various MG samples with different chemical compositions and microscopic structures display different relaxation behaviors<sup>7–11,21,32,33</sup>. Specifically, for the LaCe-based MG in this study, three different relaxation events developed during heating<sup>9</sup>. Thus, to verify whether the enlargements of the supercooled liquid region and the excess heat capacity with multiple relaxation merging via ultrafast

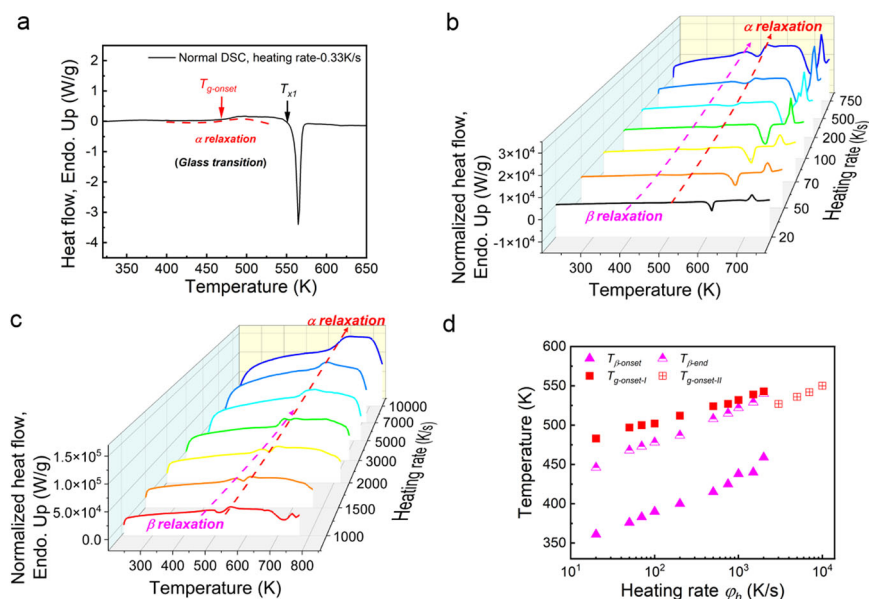


**Fig. 4** Thermodynamic and kinetic evolution with heating rates for the  $\text{La}_{60}\text{Ni}_{25}\text{Al}_{15}\text{MG}$ . **a** Heat flow curve at a heating rate of 0.33 K/s by conventional DSC for the  $\text{La}_{60}\text{Ni}_{25}\text{Al}_{15}\text{MG}$ . **b** Heat flow curves at heating rates from 20 K/s to 750 K/s by Flash DSC for the  $\text{La}_{60}\text{Ni}_{25}\text{Al}_{15}\text{MG}$ . **c** Heat flow curves at heating rates from 1000 K/s to 10,000 K/s by Flash DSC for the  $\text{La}_{60}\text{Ni}_{25}\text{Al}_{15}\text{MG}$ . **d** The evolution of the onset temperature and end temperature for the  $\beta$  relaxation and the onset temperature for the  $\alpha$  relaxation.

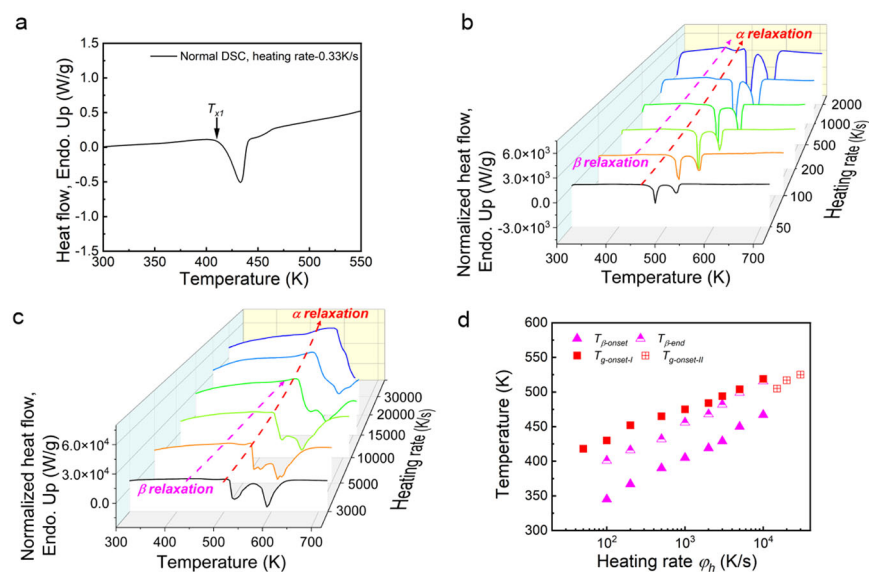
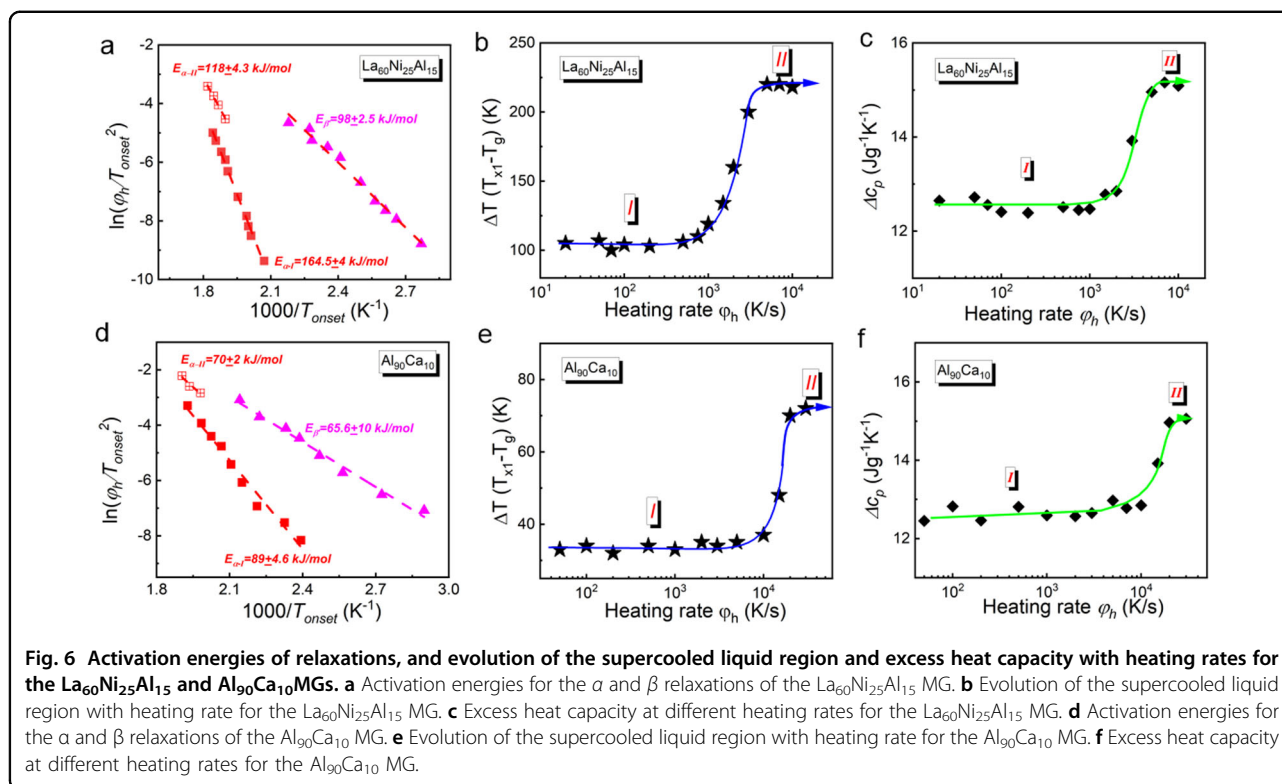


**Fig. 5** Thermodynamic and kinetic evolution with heating rates for the  $\text{Al}_{90}\text{Ca}_{10}\text{MG}$ . **a** Heat flow curve at a heating rate of 0.33 K/s by conventional DSC for the  $\text{Al}_{90}\text{Ca}_{10}\text{MG}$ . **b** Heat flow curves at heating rates from 50 K/s to 2000 K/s by Flash DSC for  $\text{Al}_{90}\text{Ca}_{10}\text{MG}$ . **c** Heat flow curves at heating rates from 3000 K/s to 30,000 K/s by Flash DSC for the  $\text{Al}_{90}\text{Ca}_{10}\text{MG}$ . **d** The evolution of the onset temperature and end temperature for the  $\beta$  relaxation and the onset temperature for the  $\alpha$  relaxation.

heating are common in MGs, two other MG systems with only the  $\beta$  relaxation were selected,  $\text{Al}_{90}\text{Ca}_{10}$  and  $\text{La}_{60}\text{Ni}_{25}\text{Al}_{15}$ ; their thermal responses under various heating rates are shown in detail in Figs. 4 and 5. For  $\text{La}_{60}\text{Ni}_{25}\text{Al}_{15}\text{MG}$ , the glass transition temperature  $T_g$  can be detected by

conventional DSC as in Fig. 4a but not for  $\text{Al}_{90}\text{Ca}_{10}\text{MG}$  (Fig. 5a). In contrast, the thermal signal corresponding to the  $\alpha$  relaxation for  $\text{Al}_{90}\text{Ca}_{10}\text{MG}$  can be observed by Flash DSC (Fig. 5b, c). For marginal MGs, such as Al-based MGs, the weak glass transition signal is prone to overlap due to



strong primary crystallization<sup>40</sup>. Thus, conventional DSC with a heating rate of only several K/s is not a suitable calorimetric measurement method to detect the glass transition of Al-based MGs. However, considering that the glass transition and crystallization are significantly different kinetic processes, they follow different evolution paths with heating rates. For higher heating rates, the thermal signals corresponding to the glass transition and crystallization evolve along two different paths, and the glass transition and crystallization separate when the heating rate increases to one critical heating rate<sup>19</sup>. Thus, the glass transition for marginal  $\text{Al}_{90}\text{Ca}_{10}$  MG can be detected by Flash DSC with a large heating rate. Moreover, compared to the LaCe-based MG with three relaxation events in Fig. 1c, only two relaxation events, the secondary  $\beta$  relaxation and the  $\alpha$  relaxation, appear in Figs. 4b, c and 5b, c. For Al-based and La-based MGs, with increasing rates of heating, the evolution rate of the  $\beta$  relaxation is much faster than that of the  $\alpha$  relaxation, and finally, the  $\beta$  relaxation and the  $\alpha$  relaxation merge when the heating rate increases to a critical value. In addition, based on the heat flow curves in Fig. 4b, c and Fig. 5b, c, the corresponding activation energies of the secondary  $\beta$  relaxation and the  $\alpha$  relaxation for the Al- and La-based MGs were calculated by fitting the Kissinger equation; the detailed values are shown in Fig. 6a and d. Similar to the LaCe-based MG, the activation energy of the  $\alpha$  relaxation decreases after the merging of the  $\beta$  relaxation and the  $\alpha$  relaxation. Moreover, the supercooled

liquid regions for the Al- and La-based MGs underwent a large increase from 34 K to 73 K and from 104 K and 221 K, respectively. These results indicate that the supercooled liquid region can be enlarged by multiple relaxation merging via ultrafast heating.

In addition, the excess heat capacity exhibited a similar step-like increase with the merging of the secondary  $\beta$  relaxation and  $\alpha$  relaxation for the La- and Al-based MGs in Fig. 6c, f. The excess heat capacity  $\Delta c_p$  increased from  $12.6 \pm 0.2 \text{ Jmol}^{-1}\text{K}^{-1}$  to  $15.2 \pm 0.1 \text{ Jmol}^{-1}\text{K}^{-1}$  and from  $12.7 \pm 0.2 \text{ Jmol}^{-1}\text{K}^{-1}$  to  $15.1 \pm 0.1 \text{ Jmol}^{-1}\text{K}^{-1}$  for the La-based and Al-based MGs, respectively. Compared to the LaCe-based MG in Fig. 3b, it is interesting to note that the increases in  $\Delta c_p$  induced by the merging of the  $\beta$  relaxation and the  $\alpha$  relaxation were very similar for all three MG systems, approximately  $2.5 \pm 0.1 \text{ Jmol}^{-1}\text{K}^{-1}$ . This result indicated that the similar value of the increase in  $\Delta c_p$  resulted from the contribution of the atomic rearrangement motions corresponding to the  $\beta$  relaxation. To illustrate the contribution of the fast relaxation to the increase in the excess heat capacity during the  $\alpha$  relaxation, a series of schemes for the heat capacity corresponding to different heating rate ranges are displayed in Fig. 3c. These schemes clearly show a common physical mechanism for the merging of the  $\beta$  relaxation and the  $\alpha$  relaxation during heating in these MG systems, which implies that different atomic rearrangement motions became more uniform with the merging of different relaxations.



## Discussion

One of the major questions in glass physics is whether vitrification from a viscous liquid into a nonequilibrium glass and devitrification from a glass to a liquid by heating are related exclusively to the primary structural relaxation process, the  $\alpha$  relaxation process, which is attributed to the cooperative motion of several structural units, or whether other atomic rearrangement motions play a role. The conventional view, based on experimental evidence for various glassy materials, indicates that the cooling rate dependence of the glass transition temperature exhibits the same behavior as the temperature dependence of viscosity or the structural  $\alpha$  relaxation time<sup>1–3</sup>. However, recent experiments on polymer glasses under geometrical confinement and MGs directly indicate that the vitrification kinetics and the  $\alpha$  relaxation are decoupled, and the role of other atomic motion mechanisms of fast relaxation play a key role<sup>31</sup>. In this work, we used Flash DSC with a heating rate range of six orders of magnitude and discovered the enlargement of the step-like supercooled liquid region enlargement and the excess heat capacity induced by multiple relaxations merging in three MGs. In particular, the increase in the excess heat capacity between the supercooled liquid and the glass during the GLT comes from the contribution of the atomic rearrangement motions corresponding to fast relaxations with the merging of the relaxation events. Therefore, these results indicate that the atomic rearrangement motions related to fast relaxation modes in addition to  $\alpha$  relaxation may be engaged in the GLT during heating at a fast heating rate.

Moreover, for glassy materials, the endothermic signals before the glass transition are actually the calorimetric features of the unfreezing of atomic rearrangement in local regions<sup>16</sup>. Here, in this work, the observed endothermic thermal signals for different relaxation events in Fig. 2a and b imply that the atomic rearrangement motions corresponding to the activation modes of multiple local structural heterogeneities in MGs are heterogeneous<sup>9,10,16,25,26</sup>. Therefore, from the viewpoint of atomic rearrangement, the merging of multiple relaxations implies the merging of different modes of atomic motion, and the atomic rearrangement during the GLT evolves from spatially heterogeneous modes to more homogeneous modes with increasing rates of heating. In addition, for the merging of relaxations with the heating rate, it is interesting to see whether these relaxations interact. If the relaxations undergo noninteraction mixing, then these relaxations may separate when the heating rate continues to increase to a critical value. Unfortunately, according to the evolution of the onset and end points of different relaxations in Figs. 2d, 4d and 5d, there are no new merging or separation behaviors after the merging of the  $\beta'$ ,  $\beta$  and  $\alpha$  relaxations for these three MG systems

within the experimental heating rate limit of the Flash DSC instrument. New calorimetric technology with a faster heating rate is needed to investigate this question. However, considering that the transition of atomic rearrangement motion with the merging of different relaxations is usually irreversible, the merging of the relaxations may be due to interaction mixing. This point will be the next focus of our research.

However, from the perspective of the potential energy landscape<sup>5,15</sup>, when the volume of the glass sample is constant, the potential energy landscape should be fixed. The energy landscape contains multiple metabasins separated by high barriers. For the relaxation events in glasses, the  $\beta$  relaxation is considered to involve stochastic and reversibly activated hopping events across “subbasins” confined within the inherent “metabasin” (intrabasin hopping), and the  $\alpha$  relaxation is considered to involve irreversible hopping events extending across different metabasins in the landscape (as shown in Fig. 1a)<sup>5</sup>. Considering the fractal nature of the potential energy landscape in glasses, the hopping barriers corresponding to the  $\alpha$  relaxation should be multiple rather than single, as indicated for a trimodal scheme at the top of Fig. 7. However, it is still unclear how a glass sample selects a corresponding energy landscape under different external stimuli. In this study, based on the above experimental results for the activation energy and the excess heat capacity for the  $\alpha$  relaxation within different heating rate ranges, three different potential energy landscapes corresponding to different heating rate ranges are displayed, as shown in Fig. 7. In the low heating rate range (stage I), the potential energy landscape displays a rough pattern with a three-level metabasin pattern as shown in Fig. 1a. In the medium heating rate range (stage II), the potential energy landscape displays a less rough pattern with a two-level metabasin pattern including the  $\beta'$  relaxation and the  $\alpha$  relaxation. In the high heating rate range (stage III), the potential energy landscape displays a smooth pattern with only a one-level pattern including the  $\alpha$  relaxation. Thus, the above evolution of the relaxation pattern with heating rate reflects the change in sampling of the potential energy landscape for MGs.

The above results for new relaxation behavior by ultrafast heating provide a new possibility to tune the relaxation pattern and enlarge the supercooled liquid region by selectively designing applied heating rates. The activated relaxation pattern and the corresponding activated energy landscape are selected according to the range of heating rate. To clearly display the evolution of the thermal relaxation spectrum, the atomic mobility heterogeneity and the activated energy landscape within different heating rate ranges, a simple scheme was proposed; it is shown in Fig. 7. Here, the atomic mobility

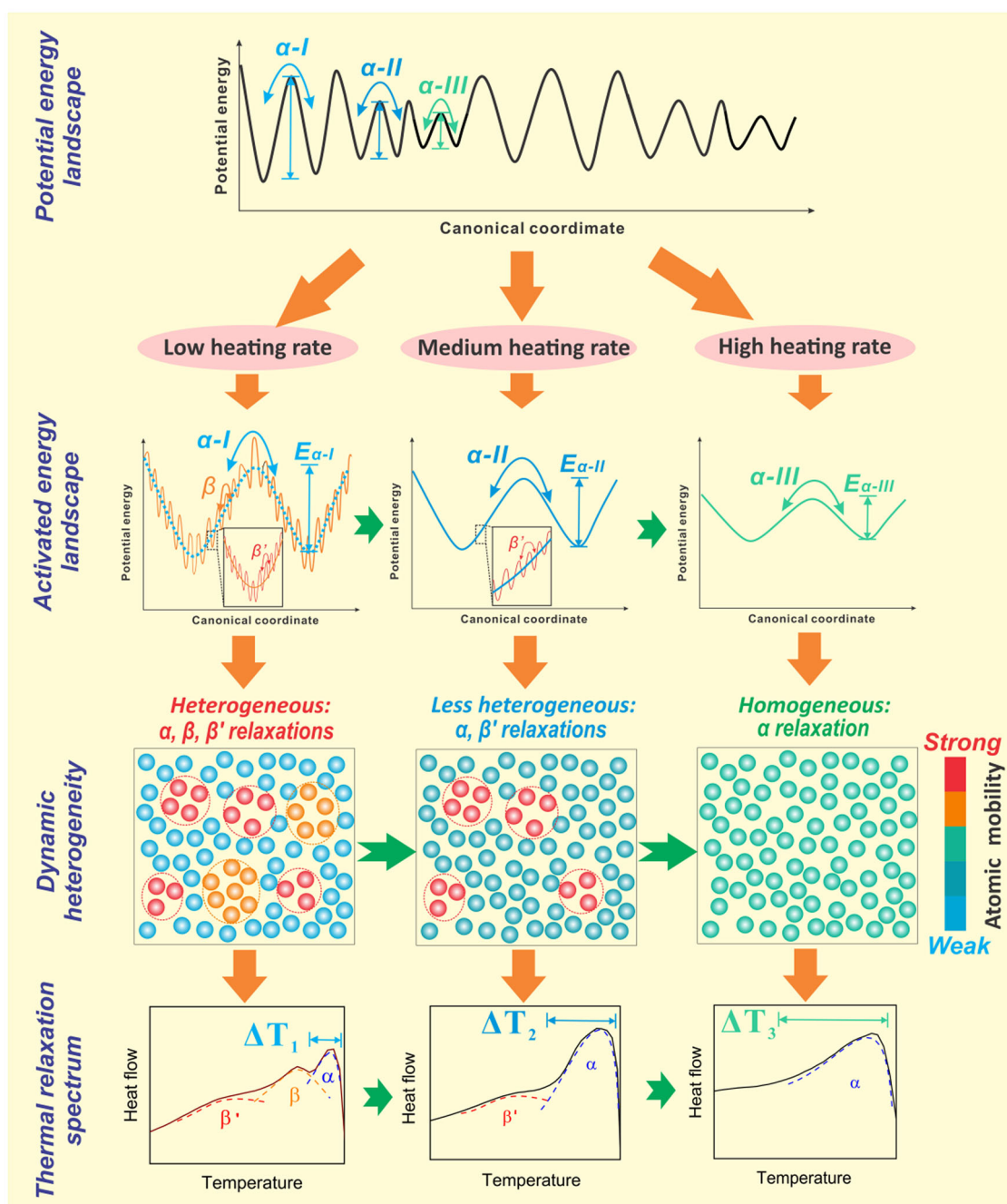


**Fig. 7** Scheme of the evolution of the thermal relaxation spectrum, atomic dynamic heterogeneity and activated energy landscape at different heating rates.

refers to the dispersion of the atomic mobility compared to the average atomic mobility at a given heating rate, which is indicated by different colors in Fig. 7. Strong atomic mobility means a larger dispersion of the atomic mobility compared to the average atomic mobility, and weak atomic mobility corresponds to a smaller dispersion of the atomic mobility compared to the average atomic

mobility. Thus, with the experimental strategy of probing the evolution of the relaxation dynamics over a larger heating rate range, new details about the potential energy landscape for a glass sample can be obtained. These new details can be extended to allow the study of the chemical composition and the effects of external stimuli on the evolution of the energy landscape.

## Conclusions

In summary, we discovered a new strategy to enlarge the supercooled liquid region of MGs by inducing the merging of multiple relaxations within a very large range of heating rates, over six orders of magnitude. We observed the step-like merging of three distinct relaxation events as the temperature and heating rate increased. The accompanying step-like increase in the excess heat capacity directly indicated that not only the atomic rearrangement motions related to the  $\alpha$  relaxation but also those related to other fast relaxations participated in the devitrification process with heating. These results provide clear experimental evidence for merging of multiple relaxations in MGs and a new understanding of the mechanism of atomic rearrangement in GLTs during heating.

## Acknowledgements

This work was supported by the Office of Naval Research of the United States (N00014-20-1-2704) and the 3315 Innovation Youth Talent Program in Ningbo City. Valuable discussions and suggestions from Prof. H. L. Peng are greatly appreciated.

## Author contributions

M.G. prepared the samples, conducted the experiments and performed the data analyses. M.G. and J.H.P. contributed to the discussion and interpretation of the results and the preparation of the manuscript.

## Conflict of interest

The authors declare no competing interests.

## Publisher's note

Springer Nature remains neutral with regard to jurisdictional claims in published maps and institutional affiliations.

Received: 13 January 2022 Revised: 8 June 2022 Accepted: 13 June 2022

Published online: 22 July 2022

## References

- Ngai, K. L. *Relaxation and Diffusion in Complex Systems* (Springer, 2011).
- Ediger, M. D., Angell, C. A. & Nagel, S. R. Supercooled liquids and glasses. *J. Phys. Chem.* **100**, 13200–13212 (1996).
- Angell, C. A., Ngai, K. L., McKenna, G. B., McMillan, P. F. & Martin, S. W. Relaxation in glass forming liquids and amorphous solids. *J. Appl. Phys.* **88**, 3113–3157 (2000).
- Dyre, J. C. Colloquium: The glass transition and elastic models of glass-forming liquids. *Rev. Mod. Phys.* **78**, 953–972 (2006).
- Debenedetti, P. G. & Stillinger, F. H. Supercooled liquids and the glass transition. *Nature* **410**, 259–267 (2001).
- Lunkenheimer, P., Schneider, U., Brand, R. & Loid, A. Glassy dynamics. *Contemp. Phys.* **41**, 15–36 (2000).
- Yu, H. B., Wang, W. H., Bai, H. Y. & Samwer, K. The  $\beta$ -relaxation in metallic glasses. *Nat. Sci. Rev.* **1**, 429–461 (2014).
- Yu, H. B., Wang, W. H. & Samwer, K. The  $\beta$  relaxation in metallic glasses: an overview. *Mater. Today* **16**, 183–191 (2013).
- Wang, Q. et al. Unusual fast secondary relaxation in metallic glass. *Nat. Comm.* **6**, 7876 (2015).
- Zhao, L. Z. et al. A fast dynamic mode in rare earth based glasses. *J. Chem. Phys.* **144**, 204507 (2016).
- Kuchenmann, S. Maaß, R. Gamma relaxation in bulk metallic glasses. *Scr. Mater.* **137**, 5–8 (2017).
- Luo, P., Wen, P., Bai, H. Y., Ruta, B. & Wang, W. H. Relaxation decoupling in metallic glasses at low temperatures. *Phys. Rev. Lett.* **118**, 225901 (2017).
- Hachenberg, J. et al. Merging of the  $\alpha$  and  $\beta$  relaxations and aging via Johari-Goldstein modes in rapidly quenched metallic glasses. *Appl. Phys. Lett.* **92**, 131911 (2008).
- Schroers, J. Processing of bulk metallic glass. *Adv. Mater.* **22**, 1566–1597 (2010).
- Wang, Z., Sun, B. A., Bai, H. Y. & Wang, W. H. Evolution of hidden localized flow during glass-to-liquid transition in metallic glass. *Nat. Comm.* **5**, 5823 (2014).
- Aji, D. P. B. & Johari, G. P. Kinetic-freezing and unfreezing of local-region fluctuations in a glass structure observed by heat capacity hysteresis. *J. Chem. Phys.* **142**, 214501 (2015).
- Schroers, J. On the formability of bulk metallic glass in its supercooled liquid state. *Acta Mater.* **56**, 471–478 (2008).
- Kumar, G., Desai, A. & Schroers, J. Bulk metallic glass: the smaller the better. *Adv. Mater.* **23**, 461–476 (2011).
- Gao, M. & Perepezko, J. H. Flash DSC determination of the delay time for primary crystallization and minor alloying effect in marginal Al-based metallic glasses. *Thermochim. Acta* **677**, 91–98 (2019).
- Gao, M. & Perepezko, J. H. Separating  $\beta$  relaxation from  $\alpha$  relaxation in fragile metallic glasses based on ultrafast flash differential scanning calorimetry. *Phys. Rev. Mater.* **4**, 025602 (2020).
- Liu, Y. H., Fujita, T., Aji, D. P. B., Matsuura, M. & Chen, M. W. Structure origins of Johari-Goldstein relaxation in a metallic glass. *Nat. Comm.* **5**, 3238 (2014).
- Lee, Jae-Chul Calorimetric study of  $\beta$ -relaxation in an amorphous alloy: an experimental technique for measuring the activation energy for shear transformation. *Intermetallics* **44**, 116–120 (2014).
- Stevenson, J. D. & Wolynes, P. G. A universal origin for secondary relaxations in supercooled liquids and structural glasses. *Nat. Phys.* **6**, 62–68 (2010).
- Karmakar, S., Dasgupta, C. & Sastry, S. Short-time beta relaxation in glass-forming liquids is cooperative in nature. *Phys. Rev. Lett.* **116**, 085701 (2016).
- Yu, H. B., Samwer, K., Wu, Y. & Wang, W. H. Correlation between  $\beta$  relaxation and self-diffusion of the smallest constituting atoms in metallic glasses. *Phys. Rev. Lett.* **109**, 095508 (2012).
- Ruta, B., Baldi, G., Monaco, G. & Chushkin, Y. Compressed correlation function and fast aging dynamics in metallic glasses. *J. Chem. Phys.* **138**, 054508 (2013).
- Zhuravlev, E. & Schick, C. Fast scanning power compensated differential scanning nano-calorimeter: 1. device. *Thermochim. Acta* **505**, 1–13 (2010).
- Zhuravlev, E. & Schick, C. Fast scanning power compensated differential scanning nano-calorimeter: 2. Heat. *Capacit. Anal., Thermochim. Acta* **505**, 14–21 (2010).
- Schick, C., Mathot, V. *Fast Scanning Calorimetry* (Springer, 2016).
- Yang, B., Schmelzer, J. W. P., Zhao, B. G., Gao, Y. L. & Schick, C. Glass transition and primary crystallization of Al86Ni6Y4.5Co2La1.5 metallic glass at heating rates spanning over six orders of magnitude. *Scr. Mater.* **162**, 146–150 (2019).
- Monnier, X., Cangialosi, D., Ruta, B., Busch, R. & Gallino, I. Vitriification decoupling from  $\alpha$ -relaxation in a metallic glass. *Sci. Adv.* **6**, 1454 (2020).
- Hu, L. N., Zhou, C., Zhang, C. Z. & Yue, Y. Z. Thermodynamic anomaly of the sub-T<sub>g</sub> relaxation in hyperquenched metallic glasses. *J. Chem. Phys.* **138**, 174508 (2013).
- Zhou, C., Yue, Y. Z. & Hu, L. N. Revealing the connection between the slow  $\beta$  relaxation and sub-T<sub>g</sub> enthalpy relaxation in metallic glasses. *J. Appl. Phys.* **120**, 225110 (2016).
- Ruitenbergh, G. Applying Kissinger analysis to the glass transition peak in amorphous metals. *Thermochim. Acta* **404**, 207–211 (2003).
- Landau, L. D., Lifshitz, E. M. *Statistical Physics* (Butterworth Heinemann, 1999).
- Adam, G. & Gibbs, J. H. On the temperature dependence of cooperative relaxation properties in glass-forming liquids. *J. Chem. Phys.* **43**, 139–146 (1965).
- Goldstein, M. Viscous liquids and the glass transition. V. sources of the excess specific heat of the liquid. *J. Chem. Phys.* **64**, 4767 (1976).
- Ke, H. B., Wen, P., Zhao, D. Q. & Wang, W. H. Correlation between dynamic flow and thermodynamic glass transition in metallic glasses. *Appl. Phys. Lett.* **96**, 251902 (2010).
- Ke, H. B., Wen, P. & Wang, W. H. The inquiry of liquids and glass transition by heat capacity. *AIP Adv.* **2**, 041404 (2012).
- Ichitsubo, T. et al. Glass-liquid transition in a less-stable metallic glass. *Phys. Rev. B* **72**, 052201 (2005).